Proceedings of 8th International Conference on Mechanical Engineering and Renewable Energy 2025
10-12 December, 2025, Chattogram, BANGLADESH

SciEn Conference Series: Engineering Vol. 4, 2026, pp 391-396 https://doi.org/10.38032/scse.2026.4.174

Study on Effect of Dimple on Aerodynamic Characteristics of NACA 0012 Airfoil

B M Saif, Sudipto Tushar Das and Gazi Faisal*

Department of Aeronautical Engineering, Military Institute of Science and Technology, Dhaka-1216, Bangladesh

ABSTRACT

This research uses FVM (Finite Volume Method) to examine the impact of profile modifications on a NACA-0012 airfoil. The profile adjustments being investigated consist of a circular dimple at the upper surface of the NACA-0012 airfoil at 50% of the chord length. This paper examines the values of coefficient of lift and drag, contours of pressure and velocity as these are the vital parameters, which are used as the parameters to do further calculations of airfoil performance, lift, drag etc. by using the k-ε model to observe the aerodynamic behaviour of the modified airfoil. Even though the airfoil's efficiency declines, the stall angle increases, causing flow separation to take longer. Validating the model is a challenge for this project. As a result, some ways to validation are used, while some other approaches are recommended for investigations in the future.

Keywords: NACA 0012 Airfoil, Dimple Effect, FVM Method, k- ε Model

1. Introduction

A slot is an aerodynamic component of an aircraft wing. Slot offers strong handling characteristics and reduces stall speed. Regardless of chord length, slots can be one or more in number and can be found in various positions, such as on the upper or lower surfaces of the wing. Slot creation is what causes the dimple (2D) effect. Airfoil dimpling delays flow separation, increases coefficient of lift (C_L), and decreases coefficient of drag (C_D).

Al-Obaidi et al. modified NACA 0012 airfoil with dimples. The velocity of the air was maintained constant (10 m/s) during the simulation using the Spalart-Allmaras turbulence model. On the upper, lower, as well as upper and lower surfaces, dimples of round, square, triangle, and elliptical at 20% of chord length were taken. The flow separation started at 20% of the chord length. The aerodynamic efficiency of the airfoil was found to increase by 6.24% at 5° angle of attack and by 3% at 10° angle of attack with the ellipse dimple [1].

In another study, the authors used a standard k-ε model with standard wall function to get the flow behaviour around the NACA 2412 airfoil with dimples in an airflow with a Reynolds number of 2×10^5. During the simulation, 2.5 mm diameter semi-circular outward and inward dimples were placed to the lower surface of the airfoil at an 80 mm chord length. The semi-circular dimples' turbulence caused a delay in the flow separation. As a result of higher lift and decreased pressure drag, the aerodynamic efficiency increased, enhancing aircraft performance. In this research, the angle of attack ranged from 0° to 12° [2].

Dimples on the upper surface of the NACA 0012 airfoil at 10%, 25%, 50% and 75% of chord length were investigated with k-ε turbulent model in the study of Saraf et al. However, the optimal place for the dimples was at 75% of the chord length. Velocity of the air was taken as 7.3 m/s. The airfoil that had dimples at 75% of the chord delayed flow separation. The coefficient of lift of the airfoil having 14° stall angle of attack was increased by 7% and coefficient of drag was reduced by 3% [3].

From 70% of the chord length to the trailing edge, 15 circular dimples with a 3 mm diameter were added to the NACA 0012 airfoil's upper surface in the study of Sandesh et al. The viscous-laminar model was used in this study. The velocity of air was kept constant during the simulation at 6 m/s. At low Reynolds numbers, the airfoil exhibited a tendency to separate the flow. The coefficient of lift of the airfoil with 10° stall angle of attack, increased with increasing angle of attack, and the same was true of the coefficient of drag [4].

The behaviour of the airflow around the NACA 0017 airfoil with dimples was simulated by some authors using an SST k-ω (shear stress transport) turbulence model. Air had a freestream velocity of 82 m/s. At 92% of the chord length, dimples of the triangle, square, and round shapes were simulated on the top and bottom surfaces. C_L decreased when the dimples were on the upper surface, and increased when they were on the lower surface. The drag only increased by 6% [5].

Using the k-ε standard turbulence model, Singh et al. simulated the flow characteristics of NACA 0012 airfoil with a rough surface at 75% of chord length. Diameter of bump was taken as 0.02C. Air velocity was kept at 7.3 m/s in the x-only direction. It was discovered that the bump caused a flow separation delay. In the direction of the trailing edge, the boundary layer thickened and separation decreased. A 12° stall angle of attack airfoil featured a high lift coefficient and reduced drag [6].

Some authors used both laminar and turbulent models to simulate the airflow around the NACA 0012 airfoil with dynamic roughness in an airflow with a Reynolds number of 100000. The separation point, which was clearly visible, was located at about 2% of the chord. There was a considerable loss of lift and reduction in drag in the airfoil having 12° stall angle of attack [7].

The conventional k-ε turbulence model was also used in a

*Corresponding Author Email Address: bmsaif1729@gmail.com

study to analyze V-shaped dimples positioned at 80% of the chord length of the NACA 0012 airfoil. Throughout the simulation, the velocity of air was maintained at 43.82 m/s. The increase in aerodynamic efficiency at angles of attack near stall at 0.8c demonstrated that the V-dimple was effective in delaying the flow separation. A V-dimpled airfoil having 12° angle of attack had a somewhat lower aerodynamic efficiency than a plain airfoil. At 14°, 16°, and 18° angles of attack, aerodynamic efficiency increased by 13.25%, 47%, and 18.24%, respectively [8].

The characteristics of the NACA 0015 airfoil with dimples having a radius of 0.006 m near the trailing edge was simulated using the SST k-turbulent model in airflow with Reynolds numbers of 2.55×10^5 and 3.6×10^5 in the study of Ismail et al. The NACA-0015 standard airfoil showed significant amounts of flow separation, but the improved airfoil had attached flow. Furthermore, because of the combined impacts of the Gurney flap and dimple, the improved airfoil generated more turbulence than the NACA-0015 base airfoil. With a slight drag penalty, the lift coefficient of the airfoil with an 18.6° stall angle of attack improved [9].

In our analysis, we have worked with the NACA 0012 airfoil with a chord length of 1000 mm. The characteristics of the airflow around the airfoil has been recorded at different angles of attack, i.e., 0°, 5°, 10°, 15°, 20°.

2. Numerical Model

2.1 The Fundamental Theory

Aerodynamic Forces

The combined effects of pressure and wall shear forces result in the drag force (F_D). Equation (1), where C_D is a drag coefficient, ρ is the density, v is the flow velocity in relation to the aircraft, and A is the wing's cross-sectional area.

$$F_D = \frac{1}{2} C_d \rho V A \tag{1}$$

$$P = \frac{1}{2} \rho C_d A V^3 \tag{2}$$

Airfoil Theories

In order to solve the compressible airflow, the Navier-Stokes equation was applied in the current work together with the k-ε turbulence model. The governing equations that form the Navier-Stokes equation include the continuity and momentum equations. The continuity equation is,

$$\frac{\partial \rho}{\partial t} + (pV) = 0 \tag{3}$$

The momentum equations in the x, y and z direction are respectively,

$$\frac{\partial \rho(uE_T)}{\partial t} + (\rho u V) = -\frac{\partial p}{\partial x} + (\mu u) + S_{m,x} \tag{4}$$

$$\frac{\partial \rho(vE_T)}{\partial t} + (\rho v V) = -\frac{\partial p}{\partial y} + (\mu v) + S_{m,y} \tag{5}$$

$$\frac{\partial \rho(wE_T)}{\partial t} + (\rho w V) = -\frac{\partial p}{\partial z} + (\mu w) + S_{m,z} \tag{6}$$

where u, v, and w are the components of velocity vector in x, y, and z-components; ρ is the air density, P_0 is static pressure, and $S_{m,x}$, $S_{m,y}$, and $S_{m,z}$ are source terms for x, y, and z components.

Governing equations of Airfoil

The normal and Axial forces on the upper surface of the airfoil are

$$dN'_u = (-p_u \cos\theta - \tau_u \sin\theta) ds_u \tag{7}$$

$$dA'_u = (-p_u \sin\theta - \tau_u \cos\theta) ds_u \tag{8}$$

The normal and Axial forces on the lower surface of the airfoil are

$$dN'_l = (p_l \cos\theta - \tau_l \sin\theta) ds_l \tag{9}$$

$$dA'_l = (p_l \sin\theta - \tau_l \cos\theta) ds_l \tag{10}$$

2.2 Turbulence Modelling

The most popular model used in computational fluid dynamics (CFD) to simulate mean flow characteristics for turbulent flow conditions is the k-ε turbulence model. There are numerous unknown and unmeasurable terms in the exact k-ε equations. The conventional k-ε turbulence model is utilized for a much more practical approach since it is based on our best understanding of the pertinent processes, minimizing unknowns and presenting a set of equations that can be used to many different turbulent situations.

For turbulent kinetic energy k,

$$\frac{\partial(\rho k)}{\partial t} + \frac{\partial(\rho u_i k)}{\partial x} = \frac{\partial}{\partial x_j}\left[\left(\mu + \frac{\mu_t}{\sigma_k}\right)\frac{\partial k}{\partial x_j}\right] + G_k + G_b - \rho \in - Y_k + S_k \tag{11}$$

For dissipation,

$$\frac{\partial(\rho \in)}{\partial t} + \frac{\partial(\rho u_i \in)}{\partial x} = \frac{\partial}{\partial x_j}\left[\left(\mu + \frac{\mu_t}{\sigma_\in}\right)\frac{\partial \in}{\partial x_j}\right] + C_{1\in}\frac{\epsilon}{k}(G_k + C_{3\epsilon} G_b) \tag{12}$$

2.3 Computational Domain

The domains of square and C are different. Frontal region coverage for the c domain exceeds the size of the rectangular domain. As we are working with various angles of attack, going beyond a particular threshold prevents us from getting the right aerodynamic behaviour of the flow around the airfoil. Therefore, c domain distributes the mesh density along the critical areas. When compared to the floor disturbance occurring in the upper and lower area of the airfoil, the frontal and rear portions of the mesh are not as crucial.

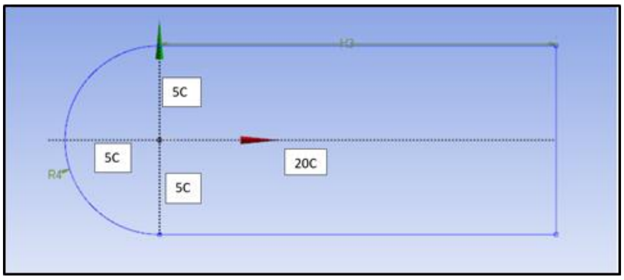

Fig. 1 Computational Domain

2.4 Meshing

A highly dense meshing has been maintained at close to the boundary by using edge sizing with a number of divisions ranging from 100 to 300 for various edges. Refinement has been taken for a denser meshing to obtain a better result. The meshed model of computational flow domain is as shown in Fig. (2-4).

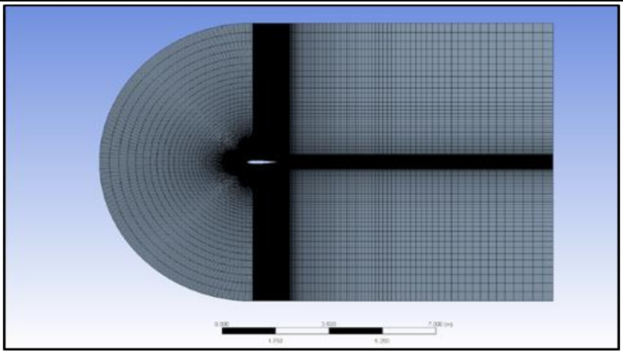

Fig 2 Structured Mesh

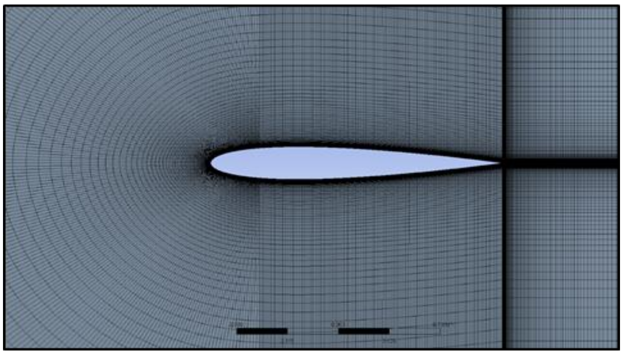

Fig 3 Near Boundary Layer Meshing

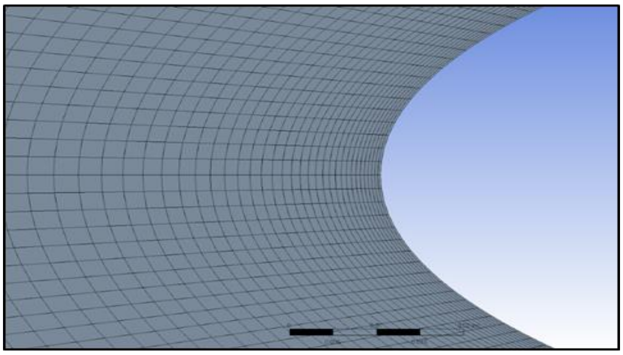

Fig 4 Sample of the Boundary Layer

2.5 Modification of Airfoil

The dimple diameter (0.05C) and its placement at 0.5C were selected to target the mid-chord region, where boundary-layer transition and flow deceleration typically begin. Positioning the dimple here should promote small-scale vortices that re-energize the boundary layer and help delay separation without causing significant geometric distortion. The chosen size provides an effective balance between flow-control strength and aerodynamic penalty.

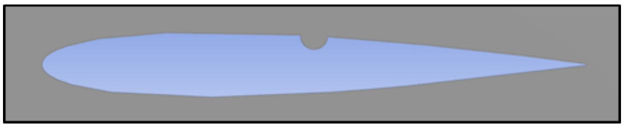

Fig 5 Sample of the Boundary Layer

2.6 Input and Boundary Conditions

The air velocity has been maintained at 50 m/s during the simulation to investigate the aerodynamic behavior of the NACA 0012 airfoil, with a chord length of 1000 mm and a maximum thickness of 0.12C, in an airflow of density 1.225 kg/m³ at angles of attack of 0°, 5°, 10°, 15°, and 20°, using the k–ε turbulence model. Inlet boundary is velocity-inlet and outlet boundary is pressure-outlet.

Table 1 Input and Boundary Conditions

Sl No.	Input	Value
1	Chord Length	1000 mm
2	Max. Thickness	0.12C
3	Velocity of Fluid	50 m/s
4	Density of Fluid	1.225 kg/m^3
5	AOA in degrees	0°, 5°, 10°, 15° & 20°
6	Turbulence Model	K-ε
7	Inlet Boundary	Velocity Inlet
8	Outlet Boundary	Pressure Outlet

2.7 Grid Independence Test

There are numerous limitations on the Grid distribution scheme. Global error is uncontrollable. However, we have some influence over local errors. The number of nodes is increased until a constant outcome is obtained in order to control this.

The outcome changes in relation to the number of nodes as we increase it. There comes a point where the results become fixed. This fixed result demonstrates that the figure's depicted number of nodes is the minimum amount we must use for our work. The maximum number of nodes used to test the grid independence are 96770. The optimum number of nodes to obtain a constant value of C_L is 48720. However, we have taken 80750 nodes in our analysis.

Table 2 Mesh Convergence Study

Number of Nodes	Coefficient of Lift
8660	1.030199
20675	1.048327
32690	1.05973
48710	1.065477
64730	1.066674
80750	1.067247
96770	1.067335

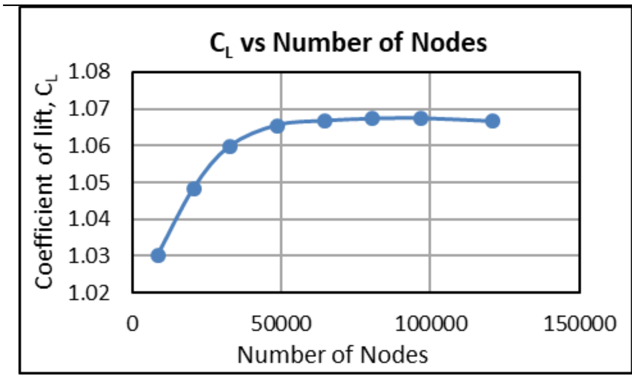

Fig 6 Grid Independence Test

2.8 The y+ Factor

A dimensionless parameter called y+ measures the ratio of turbulent to laminar effect in a cell. The first layer thickness depends on y+. When the first layer thickness is taken at a bigger value, the velocity profile may not be captured, and when the first layer thickness is taken at a lesser value, computational resources are wasted. The larger the y+ value, the more turbulent the flow. The range of y+ is between 30 and 300.

The local Reynolds number, skin friction of the airfoil, the wall shear stress, the fluid speed at the near-wall boundary and the distance to the first mesh node is calculated by equations (13-17) respectively. We measured that the value of Δy is 0.0003m.

$$Re_{Object} = \frac{p_{air} v_{air}\, l}{\mu_{air}} = \frac{1.225 \times 50 \times 1}{1.81 \times 10^{-5}} = 3.38 \times 10^{6} \quad (13)$$

$$C_f = 0.058\left(Re_{Object}^{-0.2}\right) = 0.058(3.38 \times 10^{6})^{-0.2} = 2.87 \times 10^{-3} \quad (14)$$

$$\tau_{air} = 0.5 C_f\, \rho_{air} v_{air}^2 = 0.5 \times 2.87 \times 10^{-3} \times 1.225 \times 50^2 = 4.39 \quad (15)$$

$$v^* = \sqrt{\frac{\tau_{air}}{\rho_{air}}} = \sqrt{\frac{4.395}{1.225}} = 1.894 \quad (16)$$

$$y^+ = \frac{\Delta y v^* \rho_{air}}{\mu air} = \frac{0.0003 \times 1.894 \times 1.225}{1.81 \times 10^{-5}} = 38.46 \quad (17)$$

The near-wall cell size corresponds to y+≈38.46, which falls within the log-law region and is appropriate for the realizable k−ε model with standard wall functions. The first grid point is located inside the logarithmic layer, avoiding the viscous sublayer (y+<11), where the k−ε model's wall functions lose accuracy. Grid-independence tests confirmed that further refinement of near-wall cells (increasing the number of nodes) produced negligible changes in the aerodynamic coefficients (C_L) by less than 1.5 %, which verifies that the chosen y+≈38 provides an adequate balance between accuracy and computational cost for the *k–ε* model framework.

3. Result and Discussion

3.1 Coefficient of Lift and Drag

The lift and drag performance of the NACA0012 without dimples is shown in Fig.7 and Fig.8 for various angles of attack. If the angle of attack increases, the coefficient of drag (C_D) rises. Initially, the coefficient of lift (C_L) value increases with an increase in angles of attack. After reaching 15°, the value of the coefficient of lift (C_L) suddenly starts to decline and continues to do so as the angles of attack rise. Stalling condition is the point at which the coefficient of lift value begins to decline.

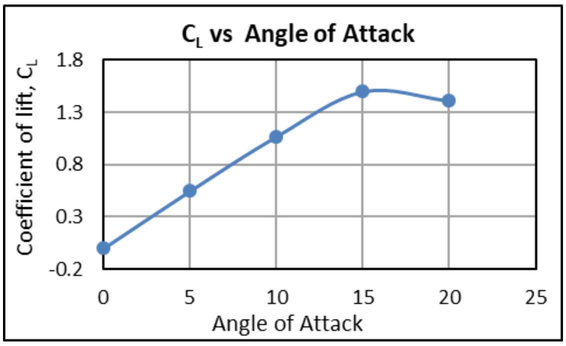

Fig 7 C_L vs AOA curve (Unmodified Airfoil)

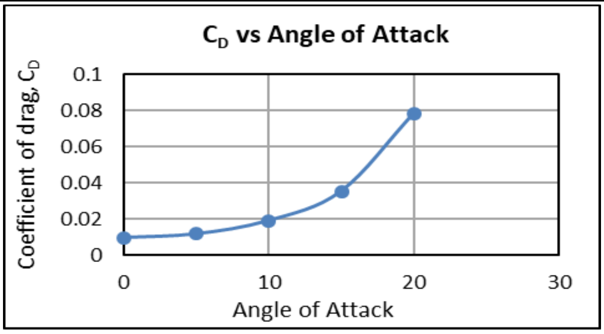

Fig 8 C_D vs AOA curve (Unmodified Airfoil)

As the angle of attack increases for the NACA0012 airfoil with dimples on the upper surface, as shown in Fig.10, the coefficient of drag increases. The nature of the coefficient of lift is likewise, as shown in Fig.9.

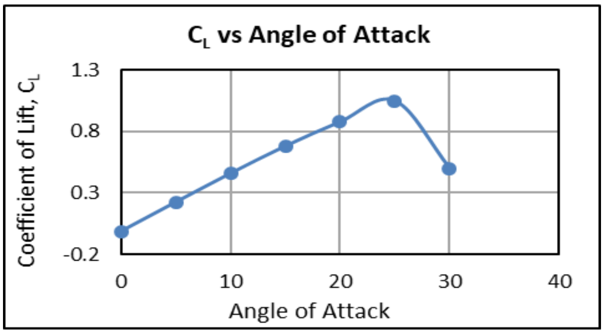

Fig 9 C_L vs AOA curve (Modified Airfoil)

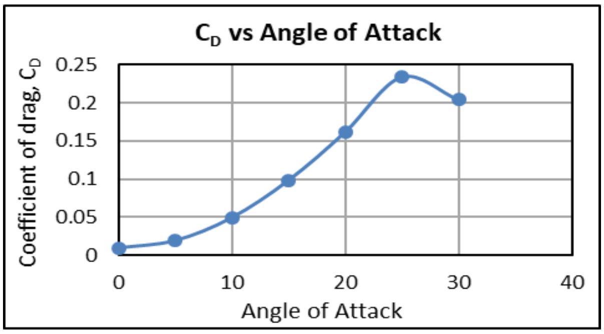

Fig 10 C_D vs AOA Curve (Modified Airfoil)

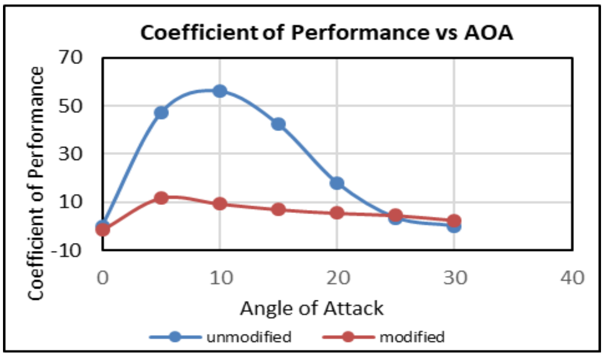

Fig 11 Coefficient of Performance vs AOA curve

The coefficient of drag values are larger for this airfoil than they are for Fig.8, which lowers the aerodynamic efficiency. Higher angles of attack result in less efficiency even if the coefficient of lift increases with angle of attack, as shown in Fig.11 and there is a possibility to increase aerodynamic performance after 25°.

For a certain AOA, the value of C_L is greater for the unmodified airfoil than modified airfoil, shown in Fig.12.

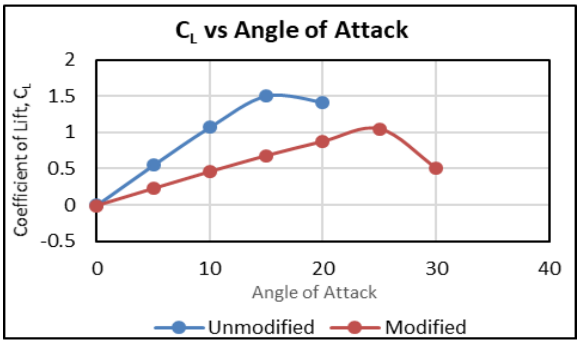

Fig 12 Comparison between C_L vs AOA

3.2 Pressure and Velocity Contour

Velocity and pressure contours for NACA 0012 modified and unmodified airfoil are observed in Fig. (13-20). The pressure contours show that the dimple at 0.5C generates localized recirculation and small vortices that energize the boundary layer, which delays separation over the aft surface. Evidence of significant local recirculation and a consequent rise in pressure drag comes from the 18% lower peak velocity. This leads to reduced overall aerodynamic efficiency. This trend agrees with previous studies [10], which reported that surface dimples delay stall but introduce a drag penalty due to pressure losses around the cavity.

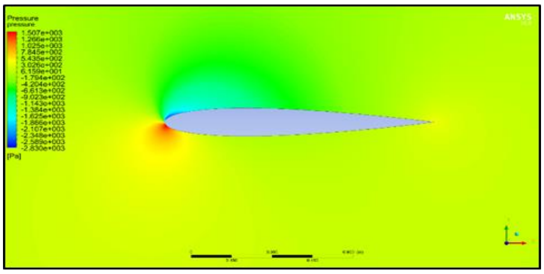

Fig 13 Pressure Contour at 5° AOA (Unmodified Airfoil)

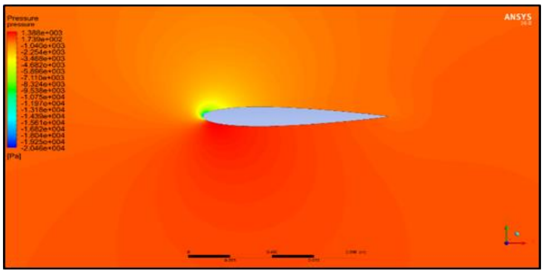

Fig 14 Pressure Contour at 20°AOA (Unmodified Airfoil)

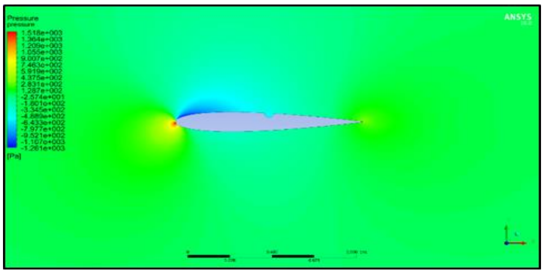

Fig 15 Pressure Contour at 5° AOA (Modified Airfoil)

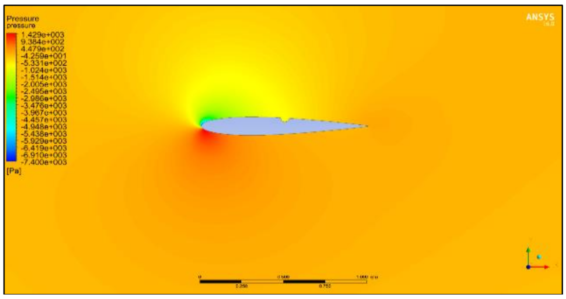

Fig 16 Pressure Contour at 20° AOA (Modified Airfoil)

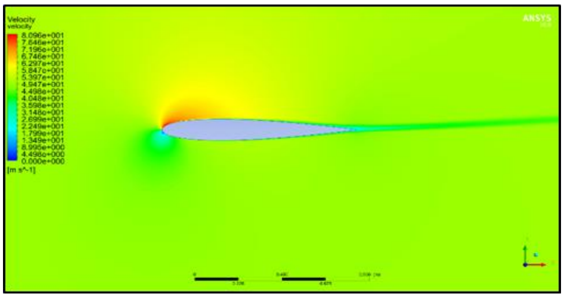

Fig 17 Velocity Contour at 5° AOA (Unmodified Airfoil)

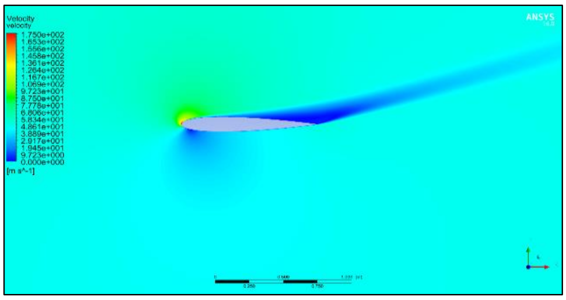

Fig 18 Velocity Contour at 20° AOA (Unmodified Airfoil)

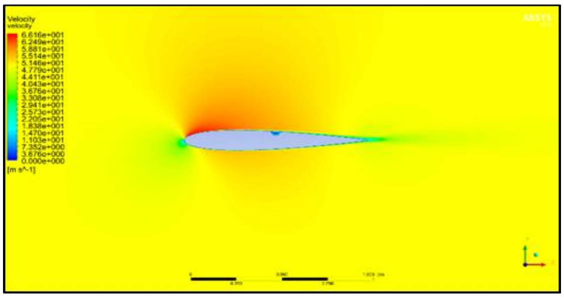

Fig 19 Velocity Contour at 5° AOA (Modified Airfoil)

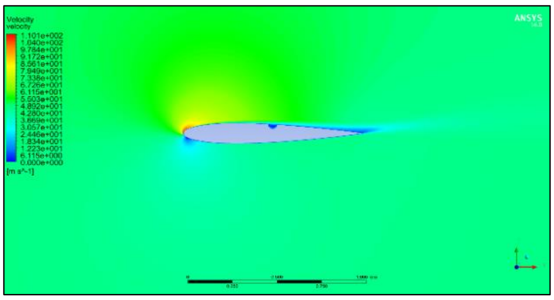

Fig 20 Velocity Contour at 20° AOA (Modified Airfoil)

3.3 Flow Separation

The dimple significantly delays flow separation. For the unmodified airfoil, flow separation occurs at an angle of attack of 15°, as shown in Fig. 21, whereas for the modified airfoil, the flow remains attached up to 25°, as shown in Fig. 22. The vortices generated by the dimple energize the boundary layer.

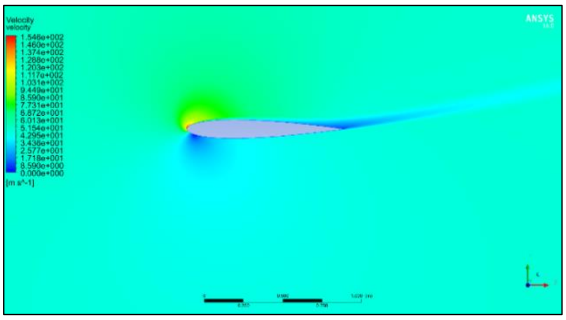

Fig 21 Flow separation at 15° AOA (Unmodified Airfoil)

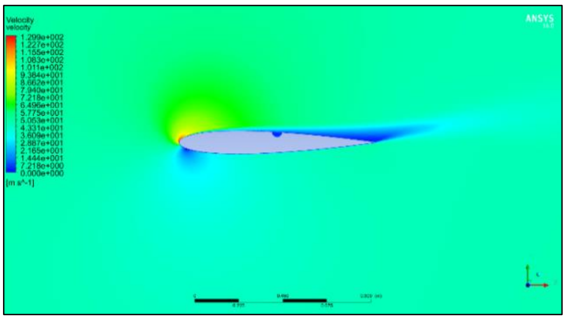

Fig 22 Flow Separation at 25° AOA (Modified Airfoil)

Although the dimple delayed flow separation by enhancing boundary-layer mixing, it also introduced additional surface roughness and recirculation losses, which increased drag and reduced overall aerodynamic efficiency. Repositioning the dimple slightly upstream (around 0.3–0.4C) or using multiple smaller dimples could improve flow reattachment while minimizing drag penalties, thereby achieving better lift-to-drag performance.

3.4 Validation of CFD Results with Benchmark Data

The CFD model was validated against established benchmark data for the baseline NACA-0012 airfoil under comparable conditions to ensure accuracy of the solver setup, turbulence model, and mesh resolution. Specifically, the simulated aerodynamic coefficients for the smooth NACA-0012 at Re = 3×10^6 were compared with the benchmark data of airfoil tools.

Table 3 Comparison between CFD Results and Benchmark Data

Parameter	**Benchmark Data**	**Present CFD**	**Deviation**
C_L slope (0–10°)	0.108/deg	0.106/deg	1.8 %
C_D @ 0°	0.0099	0.0095	4.2%
Stall angle	14.4°	15°	4.1%

The small discrepancies (≤ 5%) are within the accepted tolerance for steady-state RANS simulations using the realizable k–ε model. Furthermore, the grid-independence test confirmed that aerodynamic coefficients varied by less than 1% beyond ~1.2 million cells, verifying mesh adequacy.

4. Conclusion

For both conventional and modified airfoils, the coefficients of lift and drag were examined and compared. The coefficient of lift has decreased by 30% while the coefficient of drag has increased by 57%. Performance in terms of aerodynamics declined as a result. The flow separation has been delayed and the stalling angle of attack has increased by 10°. The dimple's position can be adjusted to be closer to the trailing edge for even greater performance. Future work will focus on optimizing dimple size, depth, and placement to improve aerodynamic efficiency while maintaining stall-delay benefits. Additional studies involving multiple dimples, advanced turbulence models, and experimental validation are planned to further understand the flow mechanisms and assess the practical applicability of the proposed modification.

5. References

[1] Soh, Z.P. and Al-Obaidi, A.S.M., 2016, December. Numerical analysis of the shape of dimple on the aerodynamic efficiency of NACA 0012 airfoil. In *Proceedings of the 6th EURECA 2016 Conference (Paper Number 2ME25), Kuala Lumpur, Malaysia* (pp. 6-7).

[2] Sowmyashree, Y., Aishwarya, D.I.P., Spurthy, S., Sah, R., Pratik, B.V., Srikanth, H.V. and Suthan, R., 2020, January. Study on effect of semi-circular dimple on aerodynamic characteristics of NACA 2412 airfoil. In *AIP Conference Proceedings* (Vol. 2204, No. 1, p. 030009). AIP Publishing LLC.

[3] Saraf, A.K., Singh, M.P. and Chouhan, T.S., 2017. Effect of dimple on aerodynamic behaviour of airfoil. *International Journal of Engineering and* Technology, *9*(3), pp.2268-2277.

[4] Rasal, S.K. and Katwate, R.R., 2017. Numerical analysis of lift & drag performance of NACA0012 wind turbine aerofoil. *International Research Journal of Engineering and Technology*, *4*(06), pp.2892-2896.

[5] Lewthwaite, M.T. and Amaechi, C.V., 2022. Numerical investigation of winglet aerodynamics and dimple effect of NACA 0017 airfoil for a freight aircraft. *Inventions*, *7*(1), p.31.

[6] Saraf, A.A.K., Singh, B.M.P. and Chouhanr, C.T.S., 2018. Study of flow separation on airfoil with bump. *International Journal of Applied Engineering Research*, *13*(16), pp.12868-12872.

[7] Huebsch, W.W., Gall, P.D., Hamburg, S.D. and Rothmayer, A.P., 2012. Dynamic roughness as a means of leading-edge separation flow control. *Journal of aircraft*, *49*(1), pp.108-115.

[8] Chullai, E.T., Singh, J., Chandel, A. and Singhal, U., 2019. Effect of V-shaped Dimples on NACA 0012 airfoil.

[9] Ismail, M.F. and Vijayaraghavan, K., 2015. The effects of aerofoil profile modification on a vertical axis wind turbine performance. *Energy*, *80*, pp.20-31.

[10] Venkatesan, S.P., Kumar, V.P., Kumar, M.S. and Kumar, S., 2018. Computational analysis of aerodynamic characteristics of dimple airfoil NACA 2412 at various angles of attack. *idea*, *46*(10).